

RSC Advances



This is an *Accepted Manuscript*, which has been through the Royal Society of Chemistry peer review process and has been accepted for publication.

Accepted Manuscripts are published online shortly after acceptance, before technical editing, formatting and proof reading. Using this free service, authors can make their results available to the community, in citable form, before we publish the edited article. This *Accepted Manuscript* will be replaced by the edited, formatted and paginated article as soon as this is available.

You can find more information about *Accepted Manuscripts* in the [Information for Authors](#).

Please note that technical editing may introduce minor changes to the text and/or graphics, which may alter content. The journal's standard [Terms & Conditions](#) and the [Ethical guidelines](#) still apply. In no event shall the Royal Society of Chemistry be held responsible for any errors or omissions in this *Accepted Manuscript* or any consequences arising from the use of any information it contains.

ARTICLE

Efficient oxidation of hydrocarbons over nanocrystalline $\text{Ce}_{1-x}\text{Sm}_x\text{O}_2$ ($x=0-0.1$) synthesized using supercritical water

Cite this: DOI: 10.1039/x0xx00000x

Received 00th January 2012,
Accepted 00th January 2012

DOI: 10.1039/x0xx00000x

www.rsc.org/

Sandip Kumar Pahari,^a Provas Pal,^a Apurba Sinhamahapatra,^a Arka Saha,^a Chiranjit Santra,^b Subhash Ch. Ghosh,^a Biswajit Chowdhury,^{b,*} and Asit Baran Panda,^{a,*}

Selective oxidation of hydrocarbons to more functional oxygenated compounds is a challenging task for industrial research. Here we report the synthesis of highly crystalline $\text{Ce}_{1-x}\text{Sm}_x\text{O}_2$ ($x=0-0.1$) using supercritical water and their excellent catalytic activity for selective oxidation of hydrocarbons (ethyl benzene, n-butylbenzene, biphenyl methane, 1,2,3,4-tetrahydro naphthalene, cyclohexene and cyclopentene) to corresponding ketone through the activation of activated proton. Materials characterization results revealed the formation of highly crystalline very small cubic nanoparticles (~ 8-10 nm) with highly exposed (100) facet and a surface area of 83-96 m^2g^{-1} . The catalytic activity results revealed that $\text{Ce}_{0.95}\text{Sm}_{0.05}\text{O}_2$ is highly active towards selective oxidation of stable sp^3 hybridized C-H bond of different hydrocarbons. The superior activity is most probably due to its high surface area, high degree of crystallinity with exposed high energy active (100) facet and presence of large amount Ce^{3+} . In optimized condition as high as 90% conversion of ethyl benzene with 87% selectivity of acetophenone was observed. Among other different substrates n-butylbenzene and cyclopentene showed 100% selectivity towards corresponding ketone with the conversion of 60% and 73% respectively. The catalyst is re-usable for minimum 5 times without any deactivation of its activity.

1. Introduction

Selective oxidation of hydrocarbons is one of the most important and essential organic transformations in modern chemical industry. Specifically, the oxidation of saturated sp^3 hybridized carbon of these hydrocarbons to corresponding oxygenated products are really challenging and most important for their tremendous economical aspect and industrial application.¹ As for instance, the acetophenone, an oxygenated product of ethyl benzene, is largely used as intermediate of some important perfumery, pharmaceutical, polymeric and fine chemical products.² Conventionally, stoichiometric oxidant, like, KMnO_4 , Ag_2O , CrO_2 , SeO_2 , and/or different Lewis acids and harsh reaction condition were used these transformations.³ All these used chemicals are costly, not recyclable and generate large amount of corrosive, noxious and pollutant wastes. Nowadays, chemical industries deserve the development of efficient catalysts which are able to provide highly atom efficient chemical reactions to reduce manufacturing costs and to minimize the burdens to the environment. In a constant search for cleaner ("greener") technologies,⁴ till date different heterogeneous and reusable catalyst has been developed for oxidation of hydrocarbon using TBHP, H_2O_2 , molecular O_2 or air as oxidant.⁵⁻⁹ Such as, Luo *et al.*⁶ reported oxidation of ethyl benzene using carbon nanotube and O_2 , Zhang *et al.*⁷ reported oxidation of hydrocarbon and alcohol using costly Nobel metal

Pd@N doped carbon and air, Chen *et al.*⁸ and Acharyya *et al.*⁹ used Co-SiO₂ based nanocomposite and CuCr_2O_4 , respectively, for ethyl benzene oxidation. However, most of developed procedure has some serious disadvantages for practical industrial applications; either the conversion and/or selectivity is not satisfactory or developed procedures used costly catalyst, such as, noble metal or carbon nanotube, transition metal based catalyst with leaching problem, high reaction temperature. Thus, a substantial development, both in catalyst and reaction condition, and conversion and selectivity, is required for practical application.

Ceria (CeO_2), important rare-earth metal oxides, is widely used as oxidation catalyst, originating from significant oxygen storage capability (OSC) and inherent $\text{Ce}^{3+}/\text{Ce}^{4+}$ red-ox cycle.¹⁰ Oxidation properties of CeO_2 is mostly controlled by $\text{Ce}^{3+}/\text{Ce}^{4+}$ redox cycle, OSC,¹¹ and the extent of these are highly controlled by size, shape, morphology and surface area. It is also reported that 10–15 nm CeO_2 nanoparticles show quantum confinement effect¹² and contain increased amount of Ce^{3+} .¹³ The creation of oxide ion defects plays a key role in designing mixed oxide catalysts.¹⁴ Among strategies for the creation of oxide ion defects, doping of CeO_2 by lower valent metal ions are the most successful strategy and Sm^{3+} doped CeO_2 shows the highest activity, since Sm^{3+} doping induces the least distortion of the parent lattice when oxygen vacancies are created in the CeO_2 lattice for charge compensation.¹⁴ Further,

it is well established that (100) surface of CeO₂ showed enhanced catalytic activity due to the higher surface energy (descending surface energy of cubic CeO₂: (100) > (110) > (111)).¹⁵ Although CeO₂ is extensively used for in automotive three-way catalysts (TWCs), and SOFC, but its use as oxidation catalyst in fine chemical synthesis is rare.

Our recent studies revealed that aqueous metal ammonium carbonate complex solutions are the novel precursor for the synthesis of nanostructure metal oxides with improved catalytic properties.¹⁶ Carbonate ions also capable to stabilize high energy facet to synthesize high energy facet exposed metal oxides.¹⁷ It has also been established that near critical and supercritical fluids are efficient and environmentally benign solvents for the rapid synthesis of metal oxide nanoparticles with high crystallinity.¹⁸ Adschiri *et al.*¹⁹ reported the decanoic acid assisted synthesis of (100) faceted cubic CeO₂, which showed improved OSC. In comprising the work of Adschiri *et al.* with our recent work, here we report the synthesis of Ce_{1-x}Sm_xO₂ (x= 0-0.1) oxide nanocrystals using corresponding cerium and samarium (Sm) ammonium carbonate complex solution under supercritical condition. The nanoparticles were characterized by XRD, BET S.A, TPR, SEM, STEM, EDX and XPS techniques. The catalytic activity of the synthesized Ce_{1-x}Sm_xO₂ catalysts were tested for liquid phase oxidation of hydrocarbons like, ethyl benzene, butyl benzene, biphenyl methane, cyclopentene, 1,2,3,4-tetrahydro naphthalene, cyclohexene, cyclohexene using H₂O₂ as an oxidant. The catalyst Ce_{0.95}Sm_{0.05}O₂ resulted maximum 90% conversion of ethyl benzene with 87% selectivity of acetophenone, and both the n-butylbenzene and cyclopentene showed 100% selectivity of corresponding ketone.

2. Experimental

2.1 Chemicals.

Ceric ammonium nitrate and ammonium carbonate were purchased from S. D. fine-chem. limited, India. Samarium nitrate and ethyl benzene, n-butylbenzene, biphenyl methane, 1,2,3,4-tetrahydro naphthalene, cyclohexene and cyclopentene were purchased from Sigma-Aldrich. All the chemicals were utilized as obtained without any additional purification. Water with a resistivity of 18MΩ cm was used for all the experiments which were obtained from a Millipore water purifier.

2.2 Synthesis of Ce_{1-x}Sm_xO₂ (x= 0-0.1) Catalyst.

The Ce_{1-x}Sm_xO₂ catalysts were synthesized by the decomposition of corresponding carbonate solution using supercritical water and the amount of Sm was varied from 2.5-10 mol% (x= 0-0.1) with respect to the total CeO₂. In a typical synthetic procedure for the synthesis of Ce_{0.95}Sm_{0.05}O₂, 4g (NH₄)₂Ce(NO₃)₆ and 0.16g Sm(NO₃)₃ 6H₂O were dissolved in 12 ml water. Around 5.6g ammonium carbonate was dissolved in 8 ml water. The mixed metal ion solution was added drop wise to the ammonium carbonate solution with constant stirring, which was resulted a clear yellow solution. Then part of the solution was transferred to a pressure-resistant Hastelloy C vessel (inner volume: 5.0 mL). A hydrothermal reaction was carried out using an electric furnace at 400 °C and 34 MPa for 15 min. The reaction was terminated by submerging the vessel in a cold water bath. After the reaction, the light yellow crystalline product was collected washed with deionised water for several times. Then the product was dried in oven at 80°C.

2.3 Synthesis of 5% Sm-CeO₂ by impregnation method.

For comparison, 5% Sm loaded CeO₂ was synthesized by normal impregnation method. For this, CeO₂ nanoparticles were synthesized by supercritical water, as mentioned in "Sec. 2.2". Required amount of Sm(NO₃)₃ 6H₂O (5 mol% Sm with respect to Ce) was dissolved in water separately and the synthesized CeO₂ was added to it. The resultant aqueous suspension was heated till dry with constant stirring. The obtained powder was calcined at 500°C for 6h.

2.3 Characterizations.

Powder X-ray diffraction patterns were recorded in the 2θ range of 20-80° on a Philips X'pert X-ray powder diffractometer using Cu Kα (λ= 1.54178 Å) radiation. The nitrogen sorption measurements were performed by using an ASAP 2010 Micromeritics, USA, at 77 K after degassing samples under vacuum (10⁻² torr) at 200 °C for 4 h. Scanning electron microscope (SEM) images were collected using Leo series 1430 VP equipped with INCA using a gold coated sample supported on aluminum stubs. Transmission electronic microscope (TEM) images were collected using a JEOL JEM 2100 microscope. X-ray photoelectron spectroscopy (XPS) was performed using a Multilab-2000 (Thermo-scientific UK) spectrometer using a monochromic MgK_α X-ray source (1256 eV) with an analyzer pass energy of 10 eV. H₂-TPR measurements were conducted on Micromeritics Autochem-II Chemisorption analyser. Details of all the characterization procedures and the method of preparing the samples have been described previously.¹⁶

2.4 Catalytic Activity Studies

All the catalytic organic reactions were performed under reflux condition using a preheated oil bath under ambient pressure in solvent free conditions with continuous stirring (400rpm) using a teflonlined magnetic needle (2.5cm long and 0.5cm outer diameter). In a typical oxidation reaction of ethyl benzene, 10 mmol of ethyl benzene, 10 wt% of catalyst with respect to substrate was taken into a 50 ml two necked round bottom flask. The reaction mixture was then heated at 120°C. When the reaction mixture seems to attain the reaction temperature, 20 mmol of 30% w/v of H₂O₂ was added slowly to the system and left for 12h. The progress of reaction was monitor by partial withdrawing of reaction mixture with certain interval of time and analysed by GC. After completion of the reaction, the catalyst was separated with the help of centrifugation and organic layer of the biphasic system was extracted by separating funnel using diethyl ether. Product was analysed by GC-MS, conversion and selectivity was obtained from GC. Tetradacane was used as internal standard. (1 mmol with respect to 10 mmol substrate). Effect of reaction parameters, such as reaction time (1-14h), reaction temperature (60-150°C), amount of catalyst (5-20w%), ratio of substrate to hydrogen peroxide (1:1-1:5), ratio of Ce to Sm have been studied. Oxidation for different hydrocarbons like, butyl benzene, 1,2,3,4-tetrahydro naphthalene, biphenyl methane, cyclopentene, cyclohexene, was performed adopting the same condition as ethyl benzene except cyclopentene, reaction was carried out at 80°C. At the end of the reaction, the catalyst was regenerated after a simple activation step and has been reused for ethyl benzene at list 5 times without significant loss in catalytic activity. The catalysts were regenerated by simple regeneration steps; separation, refluxed with 40 ml 30% (w/v)

H₂O₂ for 3 h at 80 °C with continuous stirring and drying at 120 °C for 6h.

3. Results and discussion

3.1 Characterization:

The X-ray diffraction pattern of CeO₂ and Sm-CeO₂ (Fig. 1) depict the distinct diffraction peaks, which can be indexed as (111), (200), (220), (311), (222), (400), (331) and (420) planes

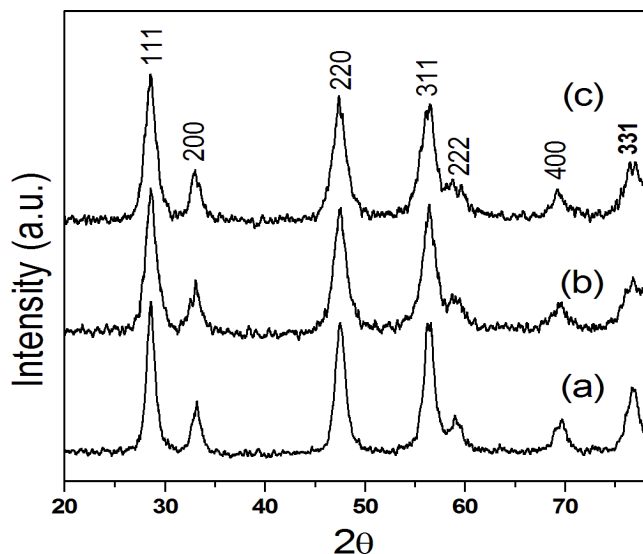


Fig. 1 Powder XRD patterns of synthesized Ce_{1-x}Sm_xO₂, where x = (a) 0, (b) 0.05 and (c) 0.1.

of cubic fluorite structure (space group: Fm3m, JCPDS 78-0694) of CeO₂. The absence of diffraction peaks for cerium hydroxide or carbonate in the XRD pattern evidenced that crystalline CeO₂ particle was formed directly from the cerium ammonium carbonate precursor solution. The peak broadening of individual reflection with the increase in Sm content in Sm incorporated samples suggested the decrease in the crystallite size. The calculated crystallite sizes, from X-ray line broadening of the (111) diffractions using Scherrer's equation, was 11.4 nm and 6.2–10.6 nm for pure CeO₂ and Sm-CeO₂, respectively (Table 1). Similar observation of the decrease in crystallite size with increase in the Sm content in Ce_{1-x}Sm_xO₂ have also been reported previously.²⁰ This phenomena may be ascribed to the decrease in concentration of surface hydroxyls due to the presence of low valent Sm³⁺ replacing the higher

Table 1 Textural and structural characteristics of the synthesized samples.

Sample	Size		a^{γ}	$S_{\text{BET}}/m^2/g^{\delta}$
	d_{XRD}^{α}	d_{TEM}^{β}		
CeO ₂	11.4	14	5.4163	79
Ce _{0.975} Sm _{0.025} O ₂	10.6	10	5.4169	87
Ce _{0.95} Sm _{0.05} O ₂	8.8	10	5.4180	95
Ce _{0.925} Sm _{0.075} O ₂	7.3	9	5.4195	97
Ce _{0.9} Sm _{0.1} O ₂	6.2–	7	5.4201	90

^αCrystallite size calculated from XRD line broadening, ^β

Particle size obtained from TEM, ^γ Unit cell parameters calculated from XRD results. ^δ BET surface area.

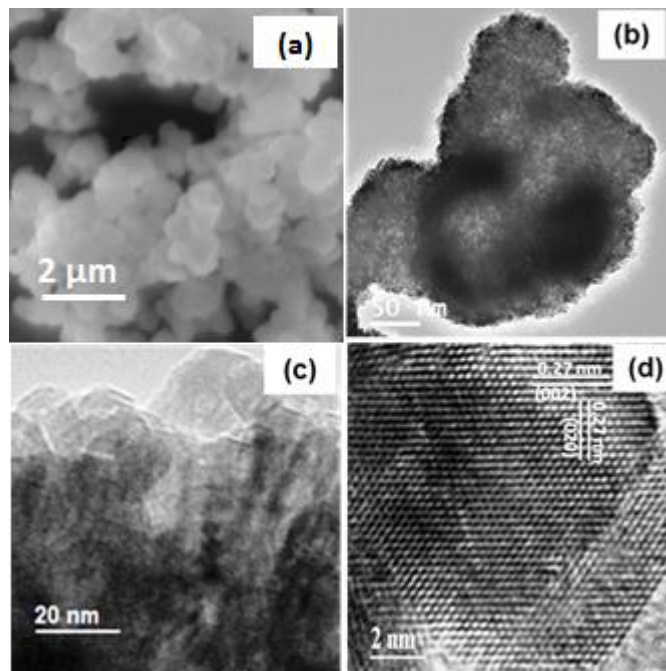


Fig. 2 (a) SEM, (b-c) TEM and (d) HR-TEM images of synthesized Ce_{0.95}Sm_{0.05}O₂.

valent Ce⁴⁺ in the CeO₂ lattice. Crystal growth took place by the dihydroxylation from two surface hydroxyl groups of neighboring nuclei and with the decrease in the surface hydroxyl group the probability of particle growth was decreased. The unit cell parameter “a” increases linearly with increasing Sm content as expected due to its enhanced effective ionic radii ($r_{\text{Ce}^{4+}} = 0.1110$ nm; $r_{\text{Sm}^{3+}} = 0.1219$ nm) (Table 1). It may be pointed out here that the diffraction lines of Ce_{1-x}Sm_xO₂ samples were shifted to lower diffraction angles with respect to the pure CeO₂. This observation can be attributed to expansion of lattices due to the replacement of Ce⁴⁺ with a larger size Sm³⁺ cation in agreement with the Vegard's rule.

Fig. 2 represents the SEM and TEM images of the synthesized Ce_{0.95}Sm_{0.05}O₂, as typical representative. SEM image (Fig. 2a) showed that the materials are spherical in nature with smooth surface. Low resolution TEM micrograph (Fig. 2b) also supports the SEM results and the synthesized materials are spherical and highly porous in nature. The magnified images depict that spheres are made of very small nanocrystals with an average particle size of ~10 nm, which are attached together to generate the porous structure (Fig. 2c). The distinct lattice fringes in HR-TEM images confirmed the formation of highly crystalline cubic particles and individual particles are single crystalline in nature (Fig. 2d). The displayed cross lattice pattern with a lattice spacing of 0.27 nm, corresponding to the interplanar distance of {002} or {020} planes, confirmed the formation of CeO₂ cubes exposing reactive (001) crystal plane.¹⁹ High angle annular dark field experiments (HADF) and STEM - x-ray energy dispersive spectroscopy (XEDX) mapping of Ce_{0.95}Sm_{0.05}O₂ (Fig. S1, ESI†) depicted the uniform dispersion of Sm atoms in the CeO₂ moiety. No discrete island of Sm was observed in the STEM-XEDS imaging. Other compositions also gave similar images. Similar to XRD crystallite size, average particle size was increased with the increase amount of Sm in the CeO₂ moiety (Table 1).

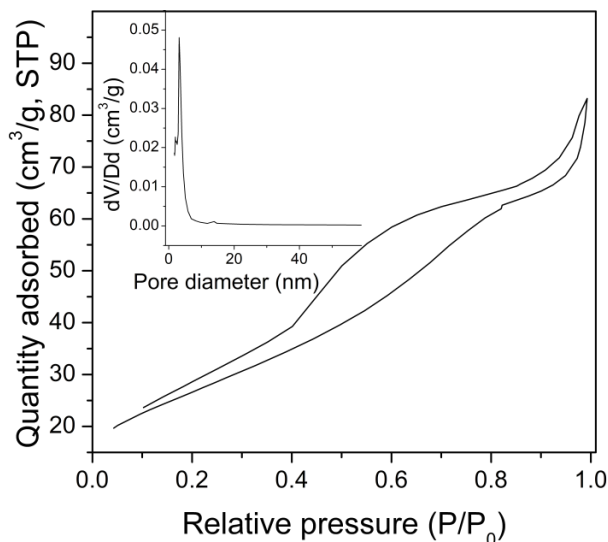


Fig. 3 N₂ adsorption–desorption isotherm of the synthesized Ce_{0.95}Sm_{0.05}O₂ material.

Nitrogen adsorption–desorption isotherm patterns correspond to type IV and mixed H2 and H3 type hysteresis loop, indicates that the synthesized nanostructure are mesoporous in nature, according to IUPAC classification (Fig. 3). As expected, the total surface area of the synthesized nanostructure is quite high, in the range of 80–95 m²/g. The pore size distribution analysis using BJH method from desorption part of the isotherm of synthesized nanostructure (inset Fig. 3) reveals a very narrow pore size distribution, with the average diameter of ~3.5 nm. The hysteresis starts from 0.37 P/P₀ regions and a distinct hysteresis in the Mid P/P₀ region of isotherm indicates presence of mesoporous structure and maximum surface area is contributed from mesoporous. Also hysteresis loop indicated nanostructured contains slit shaped particles over lapped and agglomerate with each other's forming inter-particle pores.

The Fig. 4 illustrates the 3d core level XPS spectra of CeO₂ in the region of 880–925 eV. The deconvoluted peaks (using Gaussian fit) of the 3d core level spectrum of Ce_{0.95}Sm_{0.05}O₂ in the region of 880–925 eV (Fig. 4) consist of two series of distinguishable peaks of the Ce⁴⁺ and Ce³⁺ ionic states (3d_{5/2}

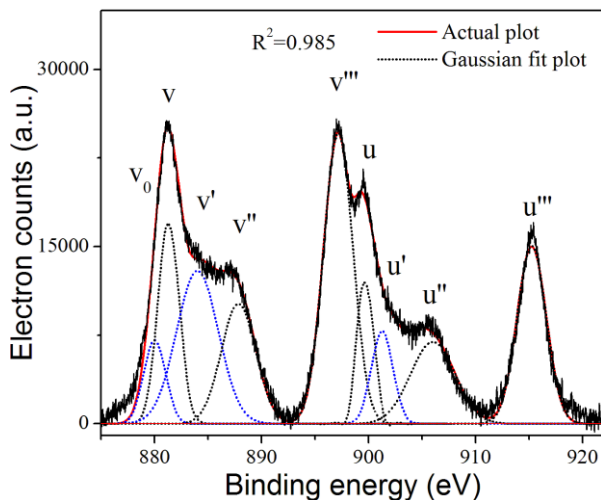


Fig. 4 Ce 3d high resolution XPS spectra of the synthesized Ce_{0.95}Sm_{0.05}O₂ nanoparticles.

and 3d_{3/2}). The deconvoluted spectrum evidenced the presence of mixed valence cerium. The peaks labeled v, v', v'', v''', u, u' and u'' were assigned to the state of Ce⁴⁺ and similarly the peaks labeled v₀ and v' and u₀, u' were assigned to the states of Ce³⁺. The semi-quantitative analysis was performed for calculation of ratio of valence states of CeO₂ present in the synthesized samples using the equation as follows,

$$[Ce^{3+}] \% = \frac{A_{v_0} + A_{v'} + A_{u_0} + A_{u'}}{A_v + A_{v''} + A_{v'''} + A_u + A_{u''} + A_{u'''}} \times 100 \%$$

where Aⁱ is the area of the corresponding peaks.

It was observed that maximum 21 % Ce³⁺ was present in the Ce_{0.95}Sm_{0.05}O₂ sample.

The H₂-TPR experiments were performed to see the change in the oxygen uptake-release capacity, i.e., redox ability, in the synthesized samples by the adopted synthetic methodology as well as on incorporation of Sm³⁺ in CeO₂ matrix. Generally two step reductions, low-temperature step for surface shell reduction at 497 °C and the high temperature step for bulk reduction 827 °C, were observed. The surface shell reduction involves (i) reduction of the surface Ce⁴⁺ to Ce³⁺; (ii) formation of bridging OH groups, where as bulk reduction involves only the reduction of Ce⁴⁺ present in core to Ce³⁺. However, in the synthesized CeO₂ both the surface and bulk reduction temperature (335°C and 443°C, respectively) decreased reasonably (Fig. 5). Further decrease in the surface and bulk reduction temperature in Ce_{1-x}Sm_xO₂ samples (311°C and

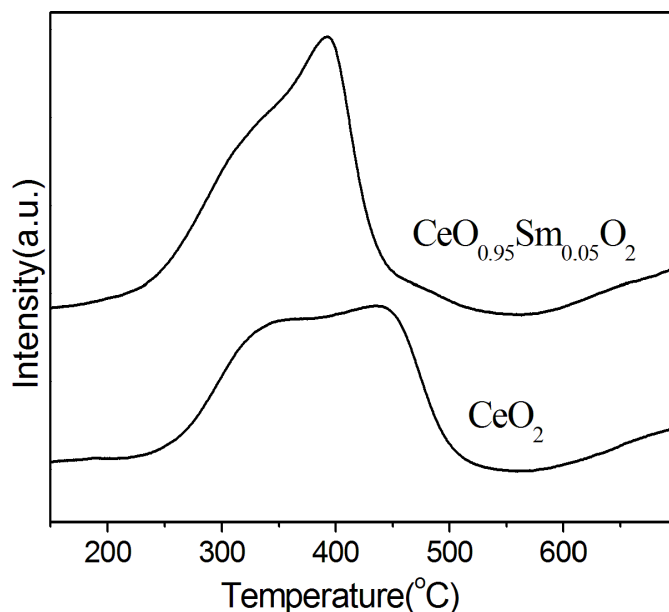


Fig. 5 H₂-TPR curves of synthesized pure CeO₂ and Ce_{0.95}Sm_{0.05}O₂ nanoparticles.

395°C, respectively for Ce_{0.95}Sm_{0.05}O₂) was observed due to incorporation of Sm³⁺ (Fig. 5) in CeO₂ lattice. Moreover the consumption of H₂ also increased with increase in the Sm content in CeO₂ moiety, e.g., for Ce_{0.95}Sm_{0.05}O₂ it is ~1.3 times more than pure CeO₂. In the nanoparticles, the surface to bulk ratio is much higher; and due to the grain surface relaxation of surface lattice²¹ and exposed active (001) surface (for the synthesized samples) the surface shell reduction temperature decreased noticeably. As bulk part is very less in nanoparticle and the existing unit cells are also quite closer to surface, so the

difference in binding energy of both (bulk and surface) oxygen is very less.

This developed strategy was based on the rapid homogeneous nucleation and growth of CeO_2 or $\text{Ce}_{1-x}\text{Sm}_x\text{O}_2$ by decomposition of clear solution of ammonium carbonate complex solution of corresponding metal ion in the oxidizing environment provided by supercritical water. In the adopted procedure all the steps such as decomposition, nucleation and growth were rapid, for which the probability for phase separation of Sm could be ruled out. Due to high temperature and pressure it formed highly crystalline nanoparticles directly. In the synthetic procedure carbonate ions may also have distinct role in selective crystal growth through (111) direction. Most probably, during the growth process carbonate ions were preferentially binds to the active (001) surface and reduce the growth rate of the crystals in $\langle 001 \rangle$ direction. As a result, crystal growth took place in $\langle 111 \rangle$ direction predominantly and lead to the formation of cubical structure with exposed (001) surface. Our recent finding on high energy {001} facet and selective synthesis of TiO_2 through stabilization of (001) surface support our probable speculation.¹⁷

3.2 Catalytic activity study.

The above mentioned characterization results confirmed that the synthesized $\text{Ce}_{1-x}\text{Sm}_x\text{O}_2$ materials with varying amount of Sm under adopted supercritical water are highly crystalline, possesses quite high surface area, reasonably large population of Ce^{3+} ions, low temperature reducible active sites, exposed active (001) plane and thus expected to be the probable suitable oxidation catalyst. So, we have targeted to use the synthesized materials as catalyst for selective oxidation of sp³ C-H bond of hydrocarbons. In the initial foot-step in this direction, we have started with the oxidation of ethyl benzene using H_2O_2 as an oxidant. At first, the oxidation of ethyl benzene was performed to screen the catalysts. The catalyst screening results, as depicted in Fig. 6 and Table-1, evidenced that the ethyl benzene conversion are almost identical for all the synthesized CeO_2 and $\text{Ce}_{1-x}\text{Sm}_x\text{O}_2$ catalysts under identical conditions, but the selectivity of acetophenone was varied with catalyst. The

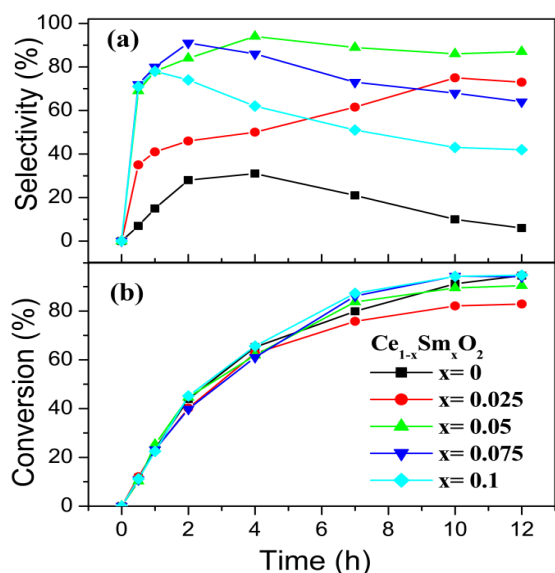


Fig. 6 Reaction profile, conversion of ethyl benzene and selectivity for acetophenone, during ethyl benzene oxidation using synthesized $\text{Ce}_{1-x}\text{Sm}_x\text{O}_2$ ($x=0, 0.025, 0.05, 0.075, 0.1$) as catalyst at 120°C , 10 wt% catalyst w. r. t. ethyl benzene.

Table 2 Catalytic activity of the synthesized $\text{Ce}_{1-x}\text{Sm}_x\text{O}_2$ catalysts for ethylbenzeneoxidation.^a

Catalyst ($\text{Ce}_{1-x}\text{Sm}_x\text{O}_2$)	^b Conv. (%)	Selectivity (%)				Y_{GC}^{c} (%)
					Other	
$x=0.00$	84	6	39	41	14	5.07
$x=0.025$	83	73	14	7	6	60.51
$x=0.05$	90	87	2	8	3	78.64
$x=0.075$	94	64	16	16	4	60.16
$x=0.1$	95	42	16	38	2	39.81
$\text{SmCeO}_2^{\text{IMP}}$	67	47	24	17	12	
CeO_2 (Bulk)	24	12	33	36	19	
Without catalyst	6	--	--	--	--	--

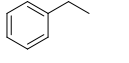
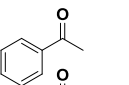
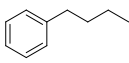
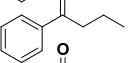
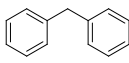
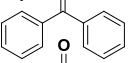
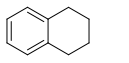
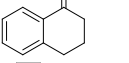
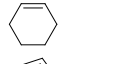
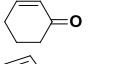
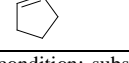
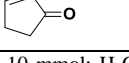
^a Typical reaction condition: 10 mmol of ethyl benzene, 10 wt% of catalyst with respect to ethyl benzene, 20 mmol of 30% w/v of H_2O_2 , reaction temperature: 120°C , reaction time: 12h; ^b Conv.: Conversion of ethyl benzene obtained from GC [(moles of ethyl benzene reacted/initial moles of ethyl benzene used) \times 100]; $\text{SmCeO}_2^{\text{IMP}}$: 5% Sm- CeO_2 catalyst prepared by impregnation method. Y_{GC}^{c} : yield of ethyl benzene obtained from GC.

selectivity of $\text{Ce}_{1-x}\text{Sm}_x\text{O}_2$ catalysts are considerably high compared to that of pure ceria and highest selectivity of acetophenone was observed for $\text{Ce}_{0.95}\text{Sm}_{0.05}\text{O}_2$ catalyst (Fig. 6). The steady increase in conversion of ethyl benzene indicates that there is no deactivation of the catalyst surface. However, after 2-3 h small decrease in the acetophenone selectivity indicated the further oxidation of acetophenone to its hydroxylated product under the employed reaction conditions. Although $\text{Ce}_{1-x}\text{Sm}_x\text{O}_2$ ($x=0.025-0.1$) is still a Ce-rich catalyst, but shows enhance activity than pure CeO_2 . $\text{Ce}_{1-x}\text{Sm}_x\text{O}_2$ ($x=0.025-0.1$) samples showed improved selectivity due to the presence of increased Ce^{3+} . Further increase in the Sm content in CeO_2 moiety selectivity of acetophenone was decreased. Hence, the observed lower selectivity of acetophenone for higher Sm content catalysts most probably due to the acceleration of the rate of decomposition of H_2O_2 to radical by Sm, which decreased the peroxo complex in the system and resist the further oxidation of phenyl alcohol to acetophenone. The role of Sm in generation of radical is well known.²² This was observed from the reaction kinetics analysis during formation of acetophenone, which takes place by the expense of 1-phenyl ethanol as observed from GC-MS analysis of stepwise evaluation of individual product (Fig. S2-S6, ESI[†]). It was observed that the 120°C and 10 wt% of catalyst is the optimized reaction temperature and amount of catalyst, respectively.

One of the most important criteria of a heterogeneous catalyst is its stability and reusability. Thus, the catalyst was reused five times after a simple regeneration steps; separation, refluxed with 40 ml 30% (w/v) H_2O_2 for 3 h at 80°C with continuous stirring and drying at 120°C for 6h. No significant change in catalytic efficiency was observed compared to fresh catalyst. After the sixth cycle, 83% conversion of ethyl benzene with a 82% selectivity for acetophenone was observed (Fig. S7, ESI[†]). The XRD and TEM results also depict that catalyst composition and morphology remained same as initial one (Fig. S8, ESI[†]).

After getting the superior activity for ethyl benzene oxidation, the $\text{Ce}_{0.95}\text{Sm}_{0.05}\text{O}_2$ was used as active catalyst oxidation of a series of hydrocarbons, such as butyl benzene, 1,2,3,4-tetrahydro naphthalene, biphenyl methane,

Table 3 oxidation of different hydrocarbons using synthesized $\text{Ce}_{0.95}\text{Sm}_{0.05}\text{O}_2$ as catalyst.^a

Entry	Reactant	Product	Conv.	Sel.
1			90	87
2			60	100
3			71	84
4			76	90
5			98	65
6			73 ^b	100

^a Reaction condition: substrate, 10 mmol; H_2O_2 , 20 mmol; catalyst, 10 wt%; temperature, 120°C; time 12h; ^b reaction temperature is 80°C; Conv.: conversion of reactant; Sel.: Selectivity of the corresponding product

cyclopentene, cyclohexene (Table 3). To our delight, $\text{Ce}_{0.95}\text{Sm}_{0.05}\text{O}_2$ also showed similar excellent catalytic activity with respect to the conversion and selectivity for all the performed hydrocarbons. Specifically, n-butylbenzene and cyclopentene showed 100% selectivity towards corresponding ketone with the conversion of 60% and 73% respectively. (Table 3).

To confirm the superiority of the synthesized nanocrystalline ceria based catalyst and to increase the selectivity of cyclohexenone, the oxidation reaction of cyclohexene was performed using $\text{Ce}_{0.95}\text{Sm}_{0.05}\text{O}_2$ catalysts synthesized by impregnation method, normal hydrothermal method and bulk CeO_2 as catalyst and without catalyst in identical optimized conditions (Table 2). The catalytic activity of the nanocrystalline $\text{Ce}_{0.95}\text{Sm}_{0.05}\text{O}_2$ catalyst synthesized by supercritical method was much higher than that of all the catalysts tested. The bulk ceria gave only 24% conversion and without catalyst only 6% conversions was observed. Even, the $\text{Ce}_{0.95}\text{Sm}_{0.05}\text{O}_2$ catalyst synthesized by hydrothermal method showed 67% conversion of cyclohexene with 47% selectivity of cyclohexenone. The activity of synthesized nanocrystalline CeO_2 is better than that of nanocrystalline CeO_2 synthesized by hydrothermal condition, vanadia supported ceria²³ and other reported catalyst (Table S1, ESI[†]). Probable origin of the superior catalytic activity of the synthesized catalyst is due to the better crystallinity, presence of enhanced amount of reducible Ce^{4+} and preferential crystal growth through (111) direction with exposed active (001) plane.

4. Conclusions

In conclusion, we report a versatile and rapid synthetic procedure for the synthesis of highly crystalline CeO_2 and Sm doped CeO_2 [$\text{Ce}_{1-x}\text{Sm}_x\text{O}_2$, $x = 0, 0.025, 0.05, 0.075, 0.1$] nanoparticles, with an average crystallite size of 7-14 nm and surface area in the range of 79-90 m^2g^{-1} using aqueous ammonium carbonate complex of Ce^{4+} and Sm^{3+} under supercritical water condition. The synthesized particles are cubic in shape with exposed active (100) plane. The doped particles are monophasic and contains reasonable amount of reducible Ce^{3+} species. The synthesized nanoparticles are highly active as oxidation catalyst towards selective oxidation

of stable sp^3 hybridized C-H bond of different hydrocarbons. Experimental results evidenced that Sm as well as extent of Sm content in CeO_2 moiety has distinct effect on catalytic activity. The catalytic activity is even better than that of other reported catalyst. The superior activity is most probably due to its high surface area, high degree of crystallinity with exposed high energy active (100) facet and presence large amount of Ce^{3+} . The catalyst is re-usable for minimum 5 times without any deactivation of its activity. Finally, the catalyst can be utilize for selective oxidation of other hydrocarbons as well as other oxidation reactions.

Acknowledgements

CSIR-CSMCRI Communication No. 37/2015. The authors are thankful to the SERB, DST, India (SR/S1/IC-33/2011) for financial support for this work. The authors also acknowledge the Analytical Discipline and Centralized Instrument Facility of CSMCRI for materials characterization.

Notes and references

^aDiscipline of Inorganic Materials and Catalysis and AcSIR, Central Salt and Marine Chemicals Research Institute (CSIR), G.B. Marg, Bhavnagar-364002, Gujarat, India. E-mail: abpanda@csmcri.org.

^bDepartment of Applied Chemistry, Indian School of Mines, Dhanbad-826004, India.

[†] Electronic Supplementary Information (ESI) available: Elemental mapping, additional catalytic results, XRD and TEM of re-used catalyst, and comparison table]. See DOI: 10.1039/b000000x/

- X. H. Li, J. S. Chen, X. C. Wang, J. H. Sun and M. Antonietti, *J. Am. Chem. Soc.*, 2011, **133**, 8074; J. A. Labinger, J. E. Bercaw, *Nature* 2002, **417**, 507; L. G.-Hortigüela, F. Corà and C. R. A. Catlow, *ACS Catal.* 2011, **1**, 1475. M. Q. Yang, Y. Zhang, N. Zhang, Z.-R. Tang and Y. J. Xu, *Sci. Reports*, 2013, **3**, 3314.
- K. George and S. Sugunan, *Catal. Commun.*, 2008, **9**, 2149; G. Y. Yang, Y. F. Ma and J. Xu, *J. Am. Chem. Soc.* 2004, **126**, 10542; J. Y. Qi, H. X. Ma, X. J. Li, Z. Y. Zhou, M. C. K. Choi, A. S. C. Chan and Q. Y. Yang, *Chem. Commun.* 2003, 1294.
- N. Chidambaram and S. Chandrasekaran, *J. Org. Chem.* 1987, **52**, 5048; T. Punniyamurthy and J. Iqbal, *Tetrahedron Lett.* 1994, **35**, 4003; J. H. Clark, A. P. Kybett, P. Landon, D. J. Macquarrie, K. Martin, *J. Chem. Soc. Chem. Commun.* 1989, 1355.
- G.-J. Brink, I.W.C.E. Arends and R.A. Sheldon, *Science* 2000, **287**, 1636.
- K. Sato, M. Aoki and R. Noyori, *Science*, 1998, **281**, 1646; T. H. Bennur, D. Srinivas and S. Sivasanker, *J. Mol. Catal. A: Chem.* 2004, **207**, 163; S. Devika, M. Palanichamy and V. Murugesan, *Appl. Catal., A* 2011, **407**, 76; V. Raji, M. Chakraborty and P. A. Parikh, *Ind. Eng. Chem. Res.* 2012, **51**, 5691; K. M. Parida and S. S. Dash, *J. Mol. Catal. A: Chem.*, 2009, **306**, 54; N. K. Mal and A. V. Ramaswamy, *Appl. Catal. A*, 1996, **143**, 75; M. Arshadi, M. Ghiaci, A. Rahmani, H. Ghaziaskar and A. Gil, *Appl. Catal. B: Env.*, 2012, **119-120**, 81; S. K. Jana, P. Wu and T. Tatsumi, *J. Catal.* 2006, **240**, 268; K. George and S. Sugunan, *Catal. Commun.*, 2008, **9**, 2149; S. Devika, M. Palanichamy, V. Murugesan, *Appl. Catal., A* 2011, **407**, 76.
- J. Luo, F. Peng, H. Yu, H. Wang and W. Zheng, *ChemCatChem*. 2013, **5**, 1578.
- P. Zhang, Y. Gong, H. Li, Z. Chen, Y. Wang, *Nature Commun.*, 2013, **4**, 1593
- C. Chen, S. Shi, M. Wang, H. Ma, L. Zhou.; J. Xu, *J. Mater. Chem. A*, 2014, **2**, 8126.

Journal Name

- 9 S. S. Acharyya, S. Ghosh, and R. Bal, *Ind. Eng. Chem. Res.* 2014, **53**, 20056.
- 10 S. Matsumoto, *Catal. Today*, 2004, **90**, 183; C. Korsvik, S. Patil, S. Seal and W. T. Self, *Chem. Commun.*, 2007, 1056; A. Trovarelli, *Catal. Rev. Sci. Eng.*, 1996, **38**, 439.
- 11 X. Liu, K. Zhou, L. Wang, B. Wang and Y. Li, *J. Am. Chem. Soc.*, 2009, **131**, 3140.
- 12 M. D. Hernandez-Alonso, A. B. Hungria, A. Martinez-Arias, J. M. Coronado, J. C. Conesa, J. Soria and M. Fernandez- Garcia, *Phys. Chem. Chem. Phys.*, 2004, **6**, 3524.
- 13 S. Tsunekawa, K. Ishikawa, Z. Q. Li, Y. Kawazoe and A. Kasuya, *Phys. Rev. Lett.*, 2000, **85**, 3440.
- 14 B. M Reddy, L. Katta, G. Thrimurthulu, *Chem. Mater.*, 2010, **22**, 467; M. Yashima and T. Takizawa *J. Phys. Chem. C*, 2010, **114**, 2385.
- 15 E. Aneggi, J. Llorca, M. Boaro and A. Trovarelli, *J. Catal.*, 2005, **234**, 88; S. Laursen, D. Combata, A. B. Hungria, M. Boronat and A. Corma, *Angew. Chem., Int. Ed.*, 2012, **51**, 4190; R. Si and M. F. Stephanopoulos, *Angew. Chem., Int. Ed.*, 2008, **47**, 2884.
- 16 N. Sutradhar, A. Sinhamahapatra, S. K. Pahari, M. Jayachandran, B. Subramanian, H. C. Bajaj and A. B. Panda, *J. Phys. Chem. C*, 2011, **115**, 7628; P. Pal, S. K. Pahari, A. Sinhamahapatra, A. K. Giri, H. C. Bajaj and A. B. Panda, *RSC Adv.*, 2013, **3**, 2802; P. Pal, S. K. Pahari, A Kanti G, S. Pal, H. C. Bajaj and A. B. Panda, *J. Mater. Chem. A*, 2013, **1**, 10251; A. Sinhamahapatra, A. K. Giri, P. Pal, S. K. Pahari, H. C. Bajaj, and A. B. Panda *J. Mater. Chem.*, 2012, **22**, 17227.
- 17 N. Sutradhar, A. K. Biswas, S. K. Pahari, B. Ganguly and A. B. Panda, *Chem. Commun.*, 2014, **50**, 11529.
- 18 T. Adschiri, Y. Hakuta, K. Sue, K. Arai, J. Nanoparticle Res., 2001, **3**, 227; A. Cabañas, J. A. Darr, E. Lester and M. Poliakoff, *J. Mater. Chem.*, 2001, **11**, 561; M. Taguchi, S. Takami, T. Adschiri, T. Nakane, K. Sato and T. Naka, *CrystEngComm*, 2012, **14**, 2132; S. K. Pahari, T. Adschiri and A. B. Panda, *J. Mater. Chem.*, 2011, **21**, 10377.
- 19 J. Zhang, S. Ohara, M. Umetsu, T. Naka, Y. Hatakeyama and T. Adschiri, *Adv. Mater.*, 2007, **19**, 203; J. Zhang, H. Kumagai, K. Yamamura, S. Ohara, S. Takami, A. Morikawa, H. Shinjoh, K. Kaneko, T. Adschiri and Akihiko Suda, *Nano Lett.* 2011, **11**, 361.
- 20 M. R. Kosinski and R. T. Baker, *J. Power Sources*, 2011, **196**, 2498.
- 21 S. Maensiri, C. Masingboon, P. Laokul, W. Jareonboon, V. Promarak, P. L. Anderson, S. Seraphin, *Cryst. Growth Des.* 2007, **7**, 950.
- 22 A. Ekstrom, J. A. Lapszewicz, *J. Am. Chem. Soc.* 1988, **110**, 5226; V. T. Amorebieta, A. J. Colussi *J. Am. Chem. Soc.* 1996, **118**, 10236.
- 23 T. Radhika, and S. Sugunan, *Catal. Commun.* 2007, **8**, 150.